Investigation of the Onset and Development of Forward Scattering in an Underdense Plasma

J. D. Moody,[1] E. A. Williams,[1] S. H. Glenzer,[1] P. E. Young,[1] J. Hawreliak,[2] A. Gouveia,[2] and J. S. Wark[2]
[1]*University of California, Lawrence Livermore National Laboratory, P. O. Box 808, Livermore, California 94550, USA*
[2]*Clarendon Laboratory, Department of Physics, University of Oxford, Oxford, OX1 3PU, United Kingdom*
(Received 17 July 2002; published 16 June 2003)

We investigate the distortion of a spatial intensity modulation imposed on a 527 nm $f/10$ probe beam as it transmits through an underdense plasma characterized with Thomson scattering. Combining the measurements with full wave simulations of beam propagation through the entire plasma show that the key features of the data can be reproduced using the Kaiser thermal transport model.

DOI: 10.1103/PhysRevLett.90.245001 PACS numbers: 52.25.Fi, 52.35.Mw, 52.38.Hb

Propagation of a high intensity laser through an underdense plasma is controlled by a complex interaction of laser-plasma physics phenomena. Stimulated scattering instabilities, inverse bremsstrahlung absorption, and passive scattering in the plasma can alter the spatial and temporal spectrum of the transmitted laser light. A number of modelers [1–3] and experimenters [4–8] have reported observations of laser-plasma instability effects on the transmitted light spatial and temporal spectrum. A systematic series of experiments measuring the resulting transmitted light modulations for a well-characterized incident laser beam and plasma would provide important information for refining existing physics descriptions of plasma thermal transport, laser-plasma instabilities, and plasma fluctuations. Progress in computational and theoretical capabilities now allows simulations in realistic mm-size plasmas [9] which make possible important tests of recent developments in nonlinear saturation [10] and nonlocal electron thermal transport models. Plasma-induced modulations on the transmitted light can also have important consequences for inertial confinement fusion (ICF). For example, the levels of forward and backward scattering may be determined as much or more by plasma modification of the incident laser light as by the characteristics of the incident laser. One possible consequence of this is that less beam conditioning may be required to mitigate scattering in ICF experiments.

In this Letter, we describe a forward scattering experiment using a well-characterized laser beam and exploding foil plasma which allowed us to determine which nonlocal electron thermal transport model best reproduces the laser forward scattering in simulations. The experiment consisted of transmitting an imposed near-field spatial intensity pattern on an interaction beam through the plasma. By varying the power of the interaction beam, we were able to systematically study the quantitative changes in the transmitted spatial pattern. The observations are reproduced in simulations using the parallel, nonlinear hydrodynamic code pF3D [11] that modeled the beam propagation through the full 1 mm plasma length of the experiment. We discovered from the model that thermal filamentation rather than ponderomotive is the primary cause of distortion to the transmitted pattern. Filamentation occurs when laser light is refracted by a local electron density depression caused by its ponderomotive pressure (ponderomotive filamentation) or from laser energy deposition (thermal filamentation). Thermal filamentation depends quantitatively on the (nonlocal) thermal conductivity and is modeled in pF3D by a Kaiser [12] or Bychencov model [13]. The Kaiser model effectively interpolates between collisional and collisionless thermal conductivity limits. The Bychencov model derives from a semirigorous solution to the linearized Fokker-Planck equation valid over the full range of collisionality. The important result is the observation that the increasing distortion of the near-field pattern with laser intensity, and the density depression created by the laser are best reproduced in simulations which use the Kaiser thermal transport model and background density fluctuations characteristic of the plasma formation beams. A Bychencov thermal model or a ponderomotive-only model do not adequately reproduce the measured results in the simulations.

Figure 1 shows the layout of the experiment conducted at the Rutherford Appleton Laboratory using seven beams of the Vulcan laser. The target plasma was formed using six heater beams of 1053 nm wavelength, 1-ns pulse length, and up to 1.2 kJ total that irradiated a 1-μm-thick CH foil. The beams were focused to a 500 μm diameter spot. Three of the beams were incident on each side of the target and overlapped along the 1 mm length of the foil uniformly illuminating an area measuring about 500 μm by 1200 μm.

The 527 nm probe beam had a 0.25-ns full-width at half-maximum (FWHM) Gaussian pulse and was delayed 0.7 ns relative to the heater beams. An $f/10$ lens focused the beam giving a 3–4 times diffraction limited FWHM spot size in vacuum measured to be ≤ 25 μm. The near-field beam without the mask had 5.4 rad of phase variation and intensity variations of less than 10% of the average intensity. The probe beam was directed along the target length transverse to the density gradient of the exploding foil where the expansion velocity is small. The beam passed through an intensity mask

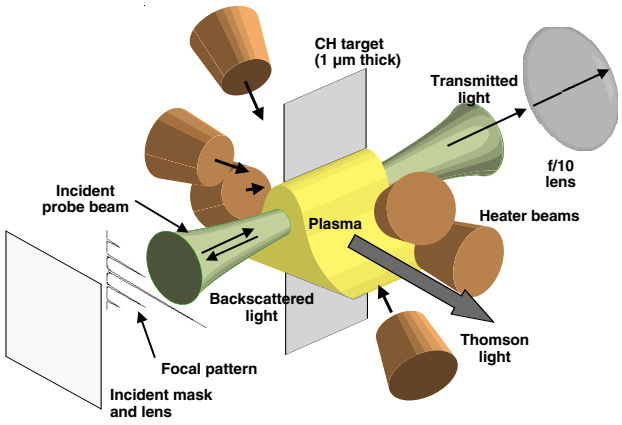

FIG. 1 (color online). Schematic layout of the experiment showing the foil illuminated by six 1053 nm beams and the 527 nm probe beam which is intensity modulated by a mask.

on the incident side of the focus lens. The purpose of the mask was to impose a well-defined transverse spatial intensity modulation on the incident beam allowing quantitative measurement of the resulting plasma-induced distortion to the mask.

The mask allowed 22% of the incident light through and consisted of a square region, measuring 10 cm along the diagonal, with a series of horizontal slit openings resembling a ''bar code'' pattern. The probe beam was polarized in the direction transverse to the mask slits. The mask pattern is a digitized binary representation of the function $[1 + 2.288\ \cos(ky)]^2$ with $k = 2\pi/0.527\ \mathrm{cm}^{-1}$ and a digitization step width of $\Delta y = 250\ \mu$m. A numerical representation of the mask is shown in Fig. 2(d). This pattern produced five vacuum focal spots aligned transverse to the density gradient and separated from each other by 100 μm with a relative intensity of 1 for the central spot, 0.3 for the two first order spots, and 0.1 for the two second order spots. The transmitted light was collected with a second $f/10$ optic. Additional optics produced a demagnified equivalent near-field mask image on a gated optical imager (GOI) with a gating time of several ns. Temporal resolution of 250 ps was achieved for both this and the Thomson scattering measurement by the probe pulse length of 250 ps.

Plasma electron and ion temperatures were diagnosed using the Thomson scattered light from the main focal spot of the incident probe beam [14]. Light collected at 80° from the probe direction was relayed to a spectrometer and recorded by a scientific CCD camera. Figure 3(a) shows the raw Thomson scattered signal resolved in wavelength and space. The Thomson data showed a slight redshift in the spectrum corresponding to a flow along the probe beam of less than 10% of the sound speed. The Thomson measurements indicate an electron temperature of 0.5 keV ± 50 eV and a local electron density normalized to the average density (n_e/n_0) along the plasma length as shown in Fig. 3(b). This density analysis takes into account the spatially

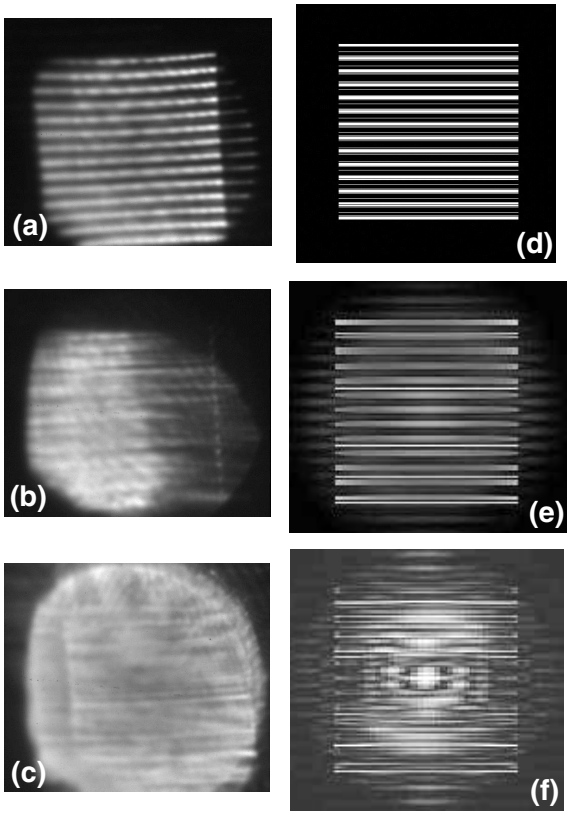

FIG. 2. The masked beam is imaged at low intensity through a vacuum in (a) and through a 1.0 mm plasma at $5 \times 10^{11}\ \mathrm{W/cm^2}$ in (b) and at $3 \times 10^{12}\ \mathrm{W/cm^2}$ in (c). (d) shows a numerical representation of the mask. pF3D simulations of the transmitted mask at $5.5 \times 10^{13}\ \mathrm{W/cm^2}$ are shown for a ponderomotive-only model in (e) and the Kaiser thermal transport plus ponderomotive in (f).

dependent probe intensity. We found that a probe beam intensity of about $5 \times 10^{14}\ \mathrm{W/cm^2}$ caused a 20% decrease in the background electron density near the position of the vacuum laser focus. Figure 3(c) shows the calculated electron density perturbation for different thermal transport models which we will discuss later. The plasma density is estimated to be 6 ± 2% critical by determining which density (with the measured electron temperature) gives the maximum calculated stimulated Raman scattering (SRS) gain at the wavelength of the measured SRS signal.

The experiment investigated the effect of increasing laser power on the transmitted spatially modulated probe beam. The probe intensity is defined to be one half of the pulse-averaged power incident on the plasma averaged over a 25 μm spot. This corresponds to approximately the intensity in the zero order spot from the mask. The 527 nm probe had a peak average intensity at the target which ranged from $3 \times 10^{11}\ \mathrm{W/cm^2}$ to $1 \times 10^{15}\ \mathrm{W/cm^2}$. Figures 2(a)–2(c) show the measured effect of the plasma on the imposed mask as the laser intensity increases. Figure 2(a) shows the mask image transmitted through the vacuum chamber with no plasma. We limited our

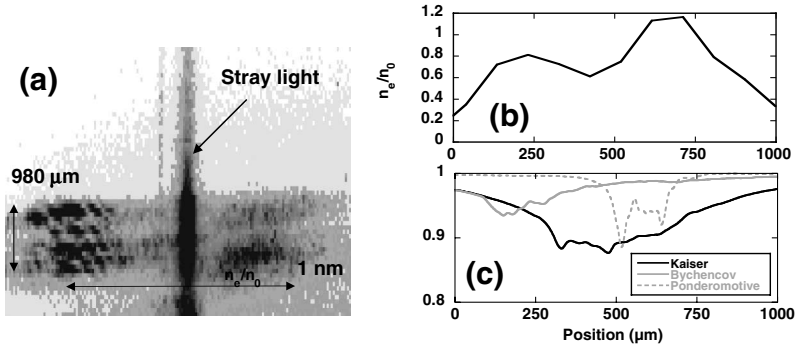

FIG. 3. (a) Spectrally and spatially resolved Thomson scattered signal shows redshifted and blueshifted emission along the length of the target. (b) The electron density (n_e) normalized to the average (n_0), obtained from the raw Thomson data, shows a 20% decrease near the plasma center. (c) Simulations using Kaiser, Bychencov, or ponderomotive-only models show differences in amplitude and location of the density perturbation.

analysis to the central and right portions of the images. Figure 2(b) shows the mask image after passing through a $6 \pm 2\%$ critical density plasma at an intensity of $5 \times 10^{11}\,\mathrm{W/cm^2}$. The large slits of the mask are still discernible and are seen to extend fairly straight and horizontally across the image indicating that refraction is not significant. The important point to make with this image is that for a sufficiently low probe power the main mask features are discernible. This establishes that it is the increase in probe intensity which affects the transmitted mask image and not the heater beam characteristics. Increasing the incident laser power further to $2.1 \times 10^{13}\,\mathrm{W/cm^2}$ shows the features of the mask becoming less distinguishable from the broad spectrum of diffuse light as can be seen in Fig. 2(c). Data at intensities above $4 \times 10^{14}\,\mathrm{W/cm^2}$ (not shown) show no detectable modulation corresponding to features of the original mask.

We quantified the effect of the plasma by analyzing the transmitted mask power spectra. The power spectra consist of a main and sometimes a second order peak superimposed on a monotonically decreasing background. The background is produced by diffusely scattered light and experimental noise. Increasing probe intensity causes the power in the spectral peaks to decrease and the diffuse part to increase. The ratio of the area under the main peak (including the diffuse signal) to the area under only the diffuse signal below the main peak is a measure of the fidelity of the main peak. The diffuse signal under the main peak is approximated by fitting a smooth monotonically decreasing curve to the diffuse signal on either side of the main peak. Figure 4 plots the fidelity of the main peak as a function of probe intensity. This value decreases as the incident intensity increases reaching a value of approximately unity at an intensity in the range of $3\text{–}8 \times 10^{13}\,\mathrm{W/cm^2}$.

We modeled the probe interaction through the entire 1 mm length of plasma with the pF3D computer model. This is a paraxial electromagnetic wave propagation model which includes plasma filamentation and forward SBS [2], backward SBS and SRS, and two nonlocal electron thermal transport models consisting of the Kaiser [12] model and a modified form of the Bychencov model [13]. The plasma is modeled as a slab with 0.5 keV electron temperature (from the Thomson data) and a 7% critical (for 527 nm light) electron density. The probe beam is modeled with its measured 5.4 rad inherent phase variations and the mask intensity modulations. Different realizations of the beam phase with similar rms do not change the simulation results. The probe passes through an $f/10$ optic and reaches focus (in vacuum) at the original center of the foil target. The goal is to test our modeling capability of laser beam propagation. The results show that our measurements are indicative of the heat transport modeling used in pF3D.

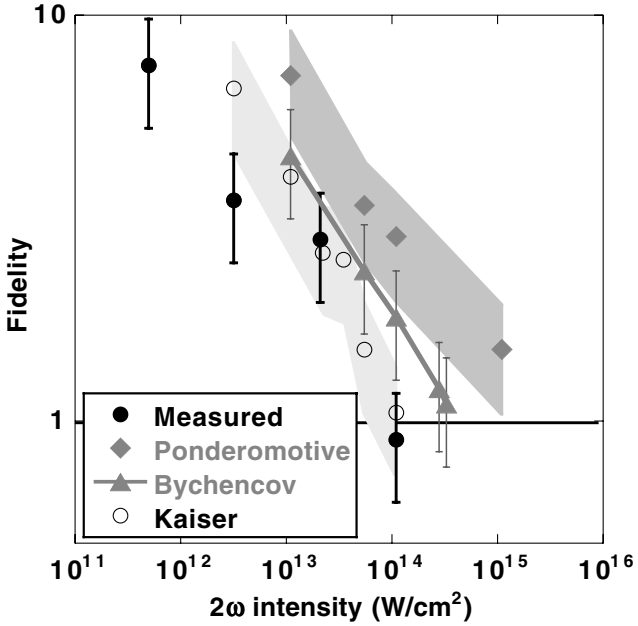

FIG. 4. Points show the fidelity of the main spectral peak in the measurement and the pF3D simulations for the ponderomotive, Bychencov, and Kaiser models.

The simulations show both a rapidly time varying and a static component to the transmitted light intensity pattern. Time averaging the transmitted intensity for 120 ps (to compare with the temporal resolution of the measurement) causes the static features to become more distinct and the rapidly changing part to become a low level of diffuse light. Figure 2 shows the results of the simulations for (e) $5.5 \times 10^{13}\,\mathrm{W/cm^2}$ with ponderomotive-only and (f) $5.5 \times 10^{13}\,\mathrm{W/cm^2}$ with ponderomotive and the Kaiser thermal model. Including nonlocal thermal effects causes a significant change in the images. Figure 4 shows the fidelity of the main peak in the power spectrum of the calculated images as a function of intensity for the ponderomotive-only, Bychencov, and Kaiser models.

We empirically accounted for experimental noise in the simulation power spectrum so that it could be directly compared with the spectrum from the measurement. This was done by adding a fixed noise power in the vicinity of the main peak of the calculated power spectrum. We chose the noise amplitude so that the main peak fidelity obtained from the measurement and simulation agreed for the case with no plasma.

Simulations using the Kaiser thermal model plus ponderomotive show the closest agreement with the measured intensity at which the fidelity becomes unity. An uncertainty in the experimental laser intensity of as much as a factor of 2 does not change this conclusion. The ponderomotive-only model shows that the intensity required for a fidelity of one is about 1 to $3 \times 10^{15}\,\mathrm{W/cm^2}$, significantly above the measured value. This result confirms that thermal effects are active and important in this plasma. Simulations using the Bychencov thermal model show a fidelity of 1 for an intensity of about 4 to $8 \times 10^{14}\,\mathrm{W/cm^2}$. This intensity is closer to but still above the measured value. We suspect that the reason the better theoretically motivated Bychencov model fails to match the data is that it cannot accurately model the thermal transport for the large temperature perturbations ($\lesssim 80\%$) observed in the simulations, underestimating the thermal conductivity when the linearization fails [15]. As a result, the laser self-focuses near the entrance to the plasma resulting in less of a distortion than predicted by the Kaiser model. The less inhibiting Kaiser thermal conductivity causes the laser spots to self-focus closer to the plasma center and produces density perturbations around the five laser focal spots which extend to several times the spot diameter. This allows perturbations from each of the five spots to overlap with adjacent spots leading to a greater distortion of the mask. Figure 3(c) shows the simulated density depression from the different models. The Kaiser model shows best agreement in location (near the vacuum laser focus) and amplitude to the density perturbation estimated from the Thomson data [Fig. 3(b)]. In contrast, the perturbation from the ponderomotive-only model is too spatially localized and the Bychencov model predicts a density perturbation that is both too small and too close to the front of the plasma. Although this comparison is only intended to be qualitative it nevertheless provides confirmation that the Kaiser model most accurately describes the nonlocal thermal transport in this plasma.

The heater beams may introduce density fluctuations in the plasma which can alter the simulation results. Modeling shows that fluctuations actually inhibit filamentation. Thus, the low intensity threshold observed in the experiment sets an upper limit on the heater beam fluctuation amplitude of $\langle \delta n/n \rangle \leq 0.01$.

In conclusion, we find that a probe beam with an imposed transverse spatial modulation is modified by forward scattering/thermal filamentation in an exploding foil plasma in an intensity-dependent manner. This experiment provides a test of the thermal transport used in the pF3D model and shows that for these plasma conditions where nonlocal thermal transport is important the basic physics of forward scattering is retained using the paraxial approximation, neglecting backscattered SRS and SBS, and incorporating the Kaiser thermal transport model. Ultimately, we expect a well-founded thermal transport model that is both nonlocal and nonlinear may be required to improve agreement with experiments in this temperature regime.

The author acknowledges useful discussion with David Chambers and help with the streak camera instruments from Roger Griffith. This experiment was carried out at the Central Laser Facility of the Rutherford Appleton Laboratory, U.K., under EPSRC Grant No. GR/L72718. This work was performed under the auspices of the U.S. Department of Energy by the Lawrence Livermore National Laboratory under Contract No. W-7405-Eng-48. This work was also partially supported by LDRD 01-LDRD-107.

[1] S. S. Coggeshall, W. C. Mead, and R. D. Jones, Phys. Fluids **31**, 2750 (1988).
[2] A. J. Schmitt and B. B. Afeyan, Phys. Plasmas **5**, 503 (1998).
[3] R. L. Berger *et al.*., Phys. Plasmas **6**, 1043 (1999).
[4] C. Labaune *et al.*, Phys. Fluids B **4**, 2224 (1992).
[5] P. E. Young, Phys. Plasmas **2**, 2815 (1995).
[6] V. V. Eliseev *et al.*, Phys. Plasmas **4**, 4333 (1997).
[7] J. D. Moody *et al.*, Phys. Rev. Lett. **83**, 1783 (1999).
[8] O. Willi *et al.*, Phys. Fluids B **2**, 1318 (1990).
[9] C. H. Still *et al.*., Phys. Plasmas **7**, 2023 (2000).
[10] S. H. Glenzer *et al.*, Phys. Rev. Lett. **86**, 2565 (2001).
[11] R. L. Berger *et al.*., Phys. Plasmas **5**, 4337 (1998).
[12] T. J. Kaiser *et al.*, Phys. Plasmas **1**, 1287 (1994).
[13] V. Bychencov *et al.*, Phys. Plasmas **7**, 1511 (2000).
[14] S. H. Glenzer *et al.*, Phys. Plasmas **6**, 2117 (1999).
[15] S. Brunner and E. Valeo, Phys. Plasmas **9**, 923 (2002).